A dWDR45 knock-out *Drosophila* model to decipher the role of autophagy in BPAN

Marion Celle[1], Sahra Aniorte[1], Abdoul Raouf Issa[1,⊥], Florence Jollivet[1], Marion Falabregue[2] Haixiu Jin[1,3], Shuze Ding[3], Laurent Seugnet[4], Lujian Liao[5], Gaetan Lesca[6,7], Ludivine Walter[1]* and Bertrand Mollereau[1]*

*co-corresponding authors

Affiliations

1-Laboratory of Biology and Modelling of the Cell, ENS of Lyon, University of Lyon, University of Claude Bernard Lyon 1, CNRS UMR 5239, INSERM U1210, UMS 3444 Biosciences Lyon Gerland, Lyon, France

2-Université Paris Cité, CNRS, INSERM,Institut Cochin, Paris, France

3-School of Physical Education and Health, East China Normal University, Shanghai, China.

4-Centre de Recherche en Neurosciences de Lyon, Team WAKING, Université Claude Bernard Lyon 1, INSERM U1028, CNRS UMR5292, Bron, France

5-Shanghai Key Laboratory of Regulatory Biology, School of Life Sciences, East China Normal University; Shanghai, 200241, China.

6-Department of Genetics, Hospices Civils de Lyon, Lyon, France

7-Neuromyogene Institute, Pathology and Genetics of neuron and muscle, CNRS UMR 5261 INSERM U1315, University of Lyon - Université Claude Bernard Lyon 1, Lyon, France

⊥ Current address: Laboratoire Plasticité du Cerveau, ESPCI-CNRS-UMR8249, INSERM-UA19, Paris, France.

Summary

Beta-propeller protein-associated neurodegeneration (BPAN) is a rare neurological disease characterized by severe cognitive and motor impairments. BPAN is caused by *de novo* pathogenic variants in the *WDR45* gene on the X chromosome. *WDR45* gene encodes the protein WDR45/WIPI4, a known regulator of autophagy. A defective autophagy has been observed in cellular models of BPAN disease and is associated with neurological dysfunctions in *WDR45* knockout (KO) mice. However, it remains unclear whether the autophagic defect directly contributes to all WDR45 loss-induced phenotypes or whether other WDR45-dependent cellular functions are involved. To investigate this, we generated a CRISPR/Cas9-mediated KO of *CG11975* (*dwdr45* KO), the *Drosophila* homolog of *WDR45*. Our analysis revealed that *dwdr45* KO flies display BPAN-like phenotypes, including impaired locomotor function, autophagy dysregulation and iron dyshomeostasis. Additionally, *dwdr45* KO flies exhibit shorten lifespan compared to control flies. These findings demonstrate that *dwdr45* KO fly is a relevant model for investigating the key cellular and molecular mechanisms underlying BPAN-associated phenotypes. Notably, induction of autophagy in *dwdr45* KO flies partially rescued the shortened lifespan, but did not restore locomotor function. This suggests that defective autophagy contributes to some, but not all, aspects of the phenotypes resulting from loss of *dwdr45* function.

Abbreviations: ATG: autophagy-related; BPAN: beta-propeller protein-associated neurodegeneration; KD: knock-down; KO: knock-out; NBIA: neurodegeneration with brain iron accumulation; WDR45: WD repeat domain 45; WIPI: WD40 repeat protein interacting with phosphoinositides.

Introduction

Beta-propeller protein-associated neurodegeneration (BPAN, MIM 300894) is a rare neurodegenerative disease caused by pathogenic variants in the autophagy-related *WDR45* gene (MIM 300526) [1]. BPAN represents the most recently identified subtype of neurodegeneration with brain iron accumulation (NBIA), and the increasing number of BPAN diagnoses in recent years positions it as a major subtype, alongside pantothenate kinase-associated neurodegeneration (PKAN). Defective autophagy has been observed in various BPAN cellular and animal models [2,3,4,5,6], although the underlying pathophysiological mechanisms remain poorly understood, and no disease-modifying treatments are currently available for BPAN patients. Thus, there is an urge to understand the cellular mechanisms underlying BPAN and identify potential cellular targets for therapeutic intervention.

Autophagy is a critical neuroprotective process that is activated in response to cellular stress to preserve neuronal health and lifespan [7,8]. Notably, pharmacological activation of autophagy has been shown to restore autophagy and alleviate cellular stress in induced pluripotent stem cell (iPSC)-derived dopaminergic neurons from BPAN patients and in *WDR45*-deficient cells, respectively [9,10]. However, it remains unclear whether the loss of WDR45-mediated autophagic regulation contributes to all BPAN-associated phenotypes.

Iron accumulation in the brain is another hallmark of BPAN, and this feature has been extensively studied in cellular models of the disease [11,12]. While iron accumulation has been reported in the brains of aged *WDR45* KO mice, other studies have failed to observe such accumulation [10,13,14]. Therefore, further investigation using additional animal models of *WDR45* deficiency is needed to study iron homeostasis in BPAN.

Drosophila melanogaster is a powerful genetic model organism for studying neurological diseases, including Parkinson's, Huntington's, and Alzheimer's diseases [15]. It is particularly well-suited for genetic studies due to its low genetic redundancy and the presence of functional orthologs/homologs for 60% to 70% of genes implicated in human diseases [16]. Moreover, autophagy and iron homeostasis mechanisms are highly conserved between flies and mammals, with key components such as ferritin proteins playing central roles in iron storage and detoxification [17,18].

In this study, we generated and characterized a *dwdr45* KO in *Drosophila* to investigate the cellular and organismal phenotypes associated with *dwdr45* loss of function. Our findings reveal multiple phenotypic manifestations reminiscent of BPAN, including impaired autophagy and iron dyshomeostasis at the cellular level, as well as motor deficits and reduced lifespan at the organismal level. Furthermore, we demonstrate that genetic activation of autophagy in *dwdr45* KO flies rescues the shortened lifespan, but does not restore locomotor dysfunction,

suggesting that dWDR45-mediated autophagy contributes to some, but not all, of the phenotypes associated with *dwdr45* loss of function.

Results

Neurological and locomotor phenotypes in *dwdr45* KO *Drosophila*

We first conducted a phylogenetic analysis comparing human WDR45/WIPI4 protein sequence with its homologs from *Homo sapiens*, *Mus musculus*, *Drosophila melanogaster*, *Caenorhabditis elegans*, and *Saccharomyces cerevisiae* (**Figure 1A**). Sequence alignment of WDR45 revealed *CG11975* as the putative *Drosophila* homolog of *WDR45*, hereafter referred to as *dwdr45*. Both the fly and human proteins share a conserved seven-blade beta-propeller, structure typical of WIPI proteins, along with conserved ATG2 interaction sites and a phosphoinositide-binding domain, known to interact with autophagy regulators (**Figure 1B, C**). Given that *WDR45* pathogenic variants are associated with severe neurological impairments in BPAN [19], we sought to examine the neuronal expression of *dwdr45* in the adult *Drosophila* brain. Using a knock-in GAL4 line, Kozak-GAL4 CG11975KO-kG4 promoter trap line combined with UAS-GFP, we tracked *dwdr45* cellular expression through the GFP labelling, and observed a widespread expression of *dwdr45* throughout the brain, with particularly strong expression in neurons marked by the anti-Elav antibody (**Figure S1**). The neuronal expression of *dwdr45* is also supported by the SCOPE single-cell sequencing data set [19,20].

To further investigate the cellular consequences of *dwdr45* deficiency, we generated a CRISPR/Cas9-mediated knockout (KO) of *dwdr45,* which is predicted to result in a null mutant. The resulting peptide is 38 amino acids in length, in contrast to the 340 amino acids of the full-length wild-type protein, and lacks the characteristic seven-blade structure as well as the autophagy regulator interaction domains (**Figure S2**).

We then assessed the locomotor phenotype of the *dwdr45* KO flies using the startle-induced negative geotaxis (SING) assay, a well-established measure of motor skills and neuronal integrity in disease models, including Parkinson's disease ([21,22] and **Figure 2A)**. In this assay, homozygous *dwdr45* KO flies exhibited a reduced performing index compared to control flies, with a further decline in performance as the flies aged, indicating progressive locomotor dysfunction (**Figure 2B**). Furthermore, knockdown of *dwdr45* using RNA interference (RNAi) under the *elav* driver also resulted in progressive locomotor deficits similar to those provoked by alpha-Synuclein overexpression, a known motor deficit inducer (**Figure S3**). Given that a locomotor decline is often associated with a loss of dopaminergic neurons across different species including flies [23], we visualized different clusters of these neurons (PAL, PPL1, PPL2, PPM1/2, and PPM3) in *dwdr45* KO flies and did not observe any neuronal loss (**Figures S4**). This could imply that neurons distinct from dopaminergic neurons are involved in the locomotion deficit observed in *dwdr45* KO flies. Importantly, pan-neuronal re-expression of wild-type *dwdr45 in dwdr45* KO flies rescued the locomotor defects in *dwdr45* KO flies (**Figure 2C**). It confirmed that the locomotor deficit is caused by *dwdr45* loss and that *dwdr45* expression in neurons is necessary for proper locomotor function in flies. In addition, We

observed similar rescue effect on the locomotion with a re-expression of human WDR45 (hWDR45) in the neurons of *dwdr45* KO (**Figure 2C**), supporting the phylogenetic analysis (**Figure 1**) and the assumption that *dwdr45* is the *Drosophila* functional homolog of human WDR45.

Fertility and lifespan reduction in *dwdr45* KO flies

In addition to the impaired locomotion, we found that homozygous *dwdr45* KO are weak fly stocks, potentially resulting from both reduced fertility and lifespan. To investigate potential fertility issues, we quantified the number of eggs laid that successfully developed into larvae, alongside counts of unfertilized (white) and nonviable (dark) eggs (**Figure 3A, B**). We observed a substantial decrease in hatching rates among homozygous *dwdr45* KO, accompanied by an increased proportion of unfertilized eggs in both heterozygous and homozygous *dwdr45* KO compared to control flies. Furthermore, *dwdr45* KO females laid over 40% of nonviable eggs, an increased number compared to both control and heterozygous *dwdr45* KO female flies. These findings suggest a fertility impairment and embryonic lethality induced by homozygous loss of *dwdr45*. To assess lifespan, we conducted longevity assays. The results revealed a nearly 50% reduction in the mean adult lifespan of heterozygous *dwdr45* KO relative to controls, while homozygous *dwdr45* KO females exhibited a severe reduction of lifespan with a mean lifespan of ≈10 days compared to ≈50 days in control flies (**Figure 3C, D, E**).

Iron dyshomeostasis in *dwdr45* KO flies

Iron dyshomeostasis has been reported in fibroblasts derived from BPAN patient tissues and in HeLa cells overexpressing mutant form of *WDR45* [24,25]. In contrast, in most cases, *WDR45* KO mouse models do not exhibit significant iron dysregulation [10,13,14]. To investigate iron homeostasis in *dwdr45* KO flies, we measured ferritin protein levels and total iron content. Ferritin status was assessed by quantifying the protein levels of Fer1HCH and Fer2LCH *via* western blotting (**Figure 4A, B, and Fig S5**). We observed elevated levels of both Fer1HCH and Fer2LCH proteins in homozygous *dwdr45* KO flies relative to controls, with Fer1HCH increase detected in newly eclosed (1-day-old) flies and Fer2LCH increase detected in 8-day-old adults.

We hypothesize that the increase in ferritin protein levels in homozygous *dwdr45* KO flies may be due to iron accumulation, a characteristic of BPAN pathology [12]. To test this hypothesis, we conducted a ferrozine assay to quantify total iron in *dwdr45* KO flies (**Figure 4C**). The results indicated a significant increase in iron content in 1-day-old homozygous *dwdr45* KO flies compared to controls, supporting the notion that *dWDR45* is essential for maintaining iron homeostasis in *Drosophila*. Together, these findings demonstrate that homozygous *dwdr45* KO flies exhibit iron dyshomeostasis, as evidenced by elevated levels of Fer1HCH, Fer2LCH, and

total iron. This aligns with BPAN pathology and provide futher validation for the *dwdr45* KO fly model.

Autophagy dysregulation in *dwdr45* KO flies

Autophagy defects have been documented in human cellular and animal models such as mouse and *Dictyostelium* models with mutations in *WDR45* or its homologs, respectively [2,26]. During the autophagy process, the accumulation of autophagic vacuoles can be detected with staining of ATG8a in flies or LC3 in mammals [27]. To assess autophagy levels, we first measured ATG8a protein accumulation by western blot using an anti-GABARAP in *Drosophila* head extracts (**Figure 5A, B**). An increase in the lipidated ATG8a-II form is commonly used as an indicator of autophagic vacuole buildup. We observed an increased ATG8a-II/ATG8a-I ratio in homozygous *dwdr45* KO compared to control flies, indicating a higher level of autophagic vacuoles. To further monitor autophagic vacuoles and assess autophagic flux in the nervous system, we examined the *Drosophila* retina, as previously described [21,28]. The pan-retinal knockdown of *dwdr45* resulted in the accumulation of GFP dots in flies expressing a transgenic GFP-LC3 construct in photoreceptor cells (**Fig. S6A,B**). The quantification of GFP-LC3 dots in the retina showed that the accumulation in *dwdr45* knockdown flies was comparable to that seen with the overexpression of the Atro75QN mutant, which has been shown to cause autophagic vacuole accumulation due to a blockage in autophagic flux in the *Drosophila* retina [28,29].

To assess autophagic flux in *dwdr45* KO flies, we examined Ref(2)P/p62, a protein that is typically degraded in autolysosomes during autophagy [28,30]. We observed an accumulation of Ref(2)P/p62 protein by western blot from *Drosophila* head extracts (**Figure 5C, D**) and by immunofluorescence in *Drosophila* retina (**Figure 5E, F**). Additionally, increased Ref(2)P was detected in retina expressing *dwdr45* RNAi, comparable to the Ref(2)P accumulation seen in retina overexpressing *Atro75QN* (**Fig. S6C, D**).

We further checked whether Ref(2)P accumulation in homozygous *dwdr45* KO retina results from impaired autophagic degradation. For this, we overexpressed GFP-Ref(2)P specifically in photoreceptors using the pan-retinal GMR driver (**Figure 5G, H**). GFP-Ref(2)P immunostaining was advantageous over endogenous Ref(2)P as it is unaffected by ROS-driven *Ref(2)P* promoter regulation [28,31], and serves as a tool to probe the autophagy dysfunction. GFP-Ref(2)P levels were significantly elevated in homozygous *dwdr45* KO retina compared to that of controls, indicating that Ref(2)P accumulation is indeed due to defective autophagy. Together, the accumulation of both ATG8a and Ref(2)P/p62 strongly suggest an impairment of autophagic flux in *dwdr45* KO flies.

Induction of autophagy improves lifespan but not locomotion deficits in *dwdr45* KO flies

Autophagy is a central mechanism to ensure neuronal health and lifespan in *Drosophila* [8,32,33]. To determine whether the observed deficits in autophagy in *dwdr45* KO flies contribute to their locomotion and lifespan phenotypes, we performed autophagy rescue experiments by overexpressing Atg1, as previously used to induce autophagy in *Drosophila* [28,34]. Notably, the pan-neuronal expression of Atg1 did not significantly improve the locomotion of *dwdr45* KO flies (**Figure 6A**). This result suggests that dWDR45 may possess an additional function, separate from autophagy, that is essential for normal locomotion. In contrast, overexpressing Atg1 was sufficient to restore lifespan in *dwdr45* KO flies (**Figure 6B-D**). Importantly, statistical analyses showed that the beneficial effect of Atg1 on lifespan was more pronounced in *dwdr45* KO flies compared to controls, supporting the idea that neuronal autophagy dysfunction plays a role in the significant lifespan reduction observed in these mutants.

Discussion

In this study, we establish a novel *Drosophila* model to study BPAN. We demonstrate that homozygous *dwdr45* KO flies display a range of cellular and behavioral phenotypes that phenocopy those observed in BPAN animal models and pathology. Specifically, *dwdr45* KO flies exhibit an autophagy dysfunction and iron accumulation at the cellular level, which correlate with locomotor impairment and reduced lifespan at the organismal level. Remarkably, pan-neuronal overexpression of Atg1, which induces autophagy, was able to extend lifespan in *dwdr45* KO flies to a further extent than in control flies, but did not improve loss of *dwdr45*-induced locomotor deficits. This finding indicates that autophagy induction can mitigate some, but not all, phenotypes associated with *dWDR45* loss of function. The lack of Atg1 overexpression on locomotion is unexpected, given autophagy's role in promoting locomotor function, as seen in *Atg5* null fly mutants [33]. We interpret this to suggest that the locomotor impairment in *dwdr45* KO flies is due to the fact that *dwdr45* in contrast to *Atg5* is not an essential gene for autophagy. This is also supported by the fact that a strong impairment of autophagy induces neurodegeneration [35], which is not observed in *dwdr45* KO flies (this study). Alternatively, an autophagy-independent role of *dwdr45* could lead to additional cellular dysfunctions, leading to locomotor impairment. Indeed, a recent study showed that *WDR45* loss triggers ATG2 recruitment to mitochondria, inducing ferroptosis *via* an autophagy-independent pathway [4]. Regarding the role of autophagy in *dwdr45* KO aging, our results show that Atg1 overexpression more effectively improves lifespan in *dwdr45* KO than in control flies, suggesting that impaired autophagy contributes to the reduced lifespan seen in *dwdr45* KO flies. The partial rescue of phenotypes by Atg1 overexpression highlights the therapeutic relevance of targeting autophagy in BPAN and also suggests the need for complementary therapies targeting non-autophagic roles of dWDR45.

Iron dysregulation remains a topic of debate in BPAN cellular and animal models. While several cellular models report iron accumulation in *WDR45*-deficient cells, measurements of ferritin levels and ferritinophagy vary across cell types [24,25,36,37]. Additionally, iron accumulation is not consistently detected in the brains of *WDR45* KO mice [10,13,14], despite being a key feature of BPAN disease. These findings suggest that iron dysregulation may occur in BPAN cellular models, but its physiological relevance in whole organisms is still unclear. The BPAN fly model exhibit increased levels of Fer1HCH and Fer2LCH associated with iron accumulation. Although it is possible that elevated ferritin levels are a consequence of reduced autophagy, namely ferritinophagy, in *dwdr45* KO flies, further study would be required to assess ferritinophagy in flies, which is beyond the scope of this work. Nevertheless, our results indicate that *dwdr45* KO flies provide a relevant model to investigate the physiological role of iron dysregulation in BPAN.

Lastly, *dWDR45* is the only homolog for both *WDR45* and *WDR45B* in mammals. The ability of human h*WDR45* to rescue the locomotion defect in *dwdr45* KO flies supports *dwdr45* KO flies as a valuable model for studying conserved functions of WDR45 in BPAN. Further research could explore the role of human WDR45B in flies, which would be highly relevant to studying neurodevelopmental pathologies associated with WDR45B mutations. Such conditions, including developmental delay, microcephaly, seizures, and neurological deterioration, partially overlap with BPAN disease phenotypes [38,39].

Materials and Methods

Drosophila culture and strains

Flies were reared on regular cornmeal-yeast medium at 25°C with a 12 h light/dark cycle. The fly stocks were obtained as followed: *CG11975*$^{KO\text{-}kG4}$ (BL97305), *UAS-GFP (on chromosome III)* [40], E*lav-Gal4 (on X)*, *UAS-WDR45.HA* (on II) (BL84770), *UAS-αSynuclein* (on III) (BL8146), *sGMR-Gal4 (on II)*, *UAS-LacZ* (on III) (BL1777) and *UAS-Atg1* (on II) (BL51654) were from Bloomington Drosophila Stock Center. *UAS-LacZ* RNAi (on II) (51446) and *UAS-dwdr45* RNAi (on III) (GD26799) were from Vienna Drosophila Resource Center. *UAS-GFP::dWDR45* (on III) was provided by P. Verstreken, *UAS-Atro75QN (on II)* was provided by M. Fanto (KCL, UK), *UAS-GFP-LC3* (on II) was provided by H. Stenmark (University of Oslo, NO) and *UAS-GFP::Ref(2)P* (on III)was provided by T. Neufeld (Universtity of Minnesota, USA).

Sequences identification and analysis

The *Drosophila* homolog of WDR45/WIPI4 was identified by performing a protein BLAST search on NCBI (https://blast.ncbi.nlm.nih.gov). To perform phylogenetic analysis, we used amino acid sequences of homologs and orthologs of WDR45/WIPI4 in *Homo sapiens*, *Mus musculus*, *Drosophila melanogaster*, *Dictyostelium discoideum* and *Saccharomyces cerevisiae* to analyze multiple sequence alignment using ClustalX with SeaView software. To define the evolutionary relationship, the phylogenetic tree was constructed using the PhyML method on SeaView software. A schematic representation of the 3D structures colorized depending on sequence conservation was created using ChimeraW software with 3D structures of *WDR45* and *dWDR45* downloaded from Swiss-Model, and sequence alignment previously performed in SeaView software.

Generation of *dwdr45* KO flies and genotyping

To generate whole body *dwdr45* KO mutant flies, we used TRIP-CRISPR lines from Bloomington Drosophila Stock Center. Firstly, flies expressing Cas9 in germline cells through nanos driver (BL54593) were crossed with flies expressing *dwdr45* guide RNA (BL83546). The expression of both guide RNA and Cas9 in first progeny (F1) males induces a deletion at position 222 of *dwdr45* gene in germline cells. To obtain whole body *dwdr45*$^{+/-}$ mutant flies, F1 males were then crossed with flies carrying TM6B,Tb balancer 50 flies were collected from this second progeny (F2) which were individually crossed with balanced flies to eliminate Cas9 and guide RNA transgene.

To confirm *dwdr45* deletion, genotyping was realized for each crosses. After genomic DNA extraction, *dwdr45* gene was amplified using touchdown PCR using the following primers: forward 5'-CATATGGAAACGGGCTGCTC-3', reverse 5'-ATCCCACACGATCACCTTG-3'.

Since *dwdr45* guide RNA targets the digestion site of BsaWI enzyme, DNA with Cas9-mediated deletion lacks this restriction site. Therefore, DNA fragments without cleavage after digestion by BsaWI were extracted from fly carrying *dwdr45* mutation. When *dwdr45* mutation was confirmed, *dwdr45* gene was sequenced to identify the precise deletion. We selected flies carrying a deletion of 7 nucleotides from nucleotide 222 to 229. This deletion induces a frameshift and a premature stop codon leading to a protein of 38 amino acids. This protein is predicted to be non functional due to the loss of the seven-beta blade-propeller structure and the loss of interaction domain with autophagy key regulators. Finally, to cross out guide RNA and Cas9 transgenic constructs, flies were crossed multiple times with flies carrying TM6B,Tb balancer.

Adult brain immunostaining

Brains from 8-day-old adult female flies were dissected in Schneider medium (Thermo Fisher Scientific, 21720001) and stored in Schneider + 1% paraformaldehyde (PFA [Euromedex, EM-15710]) until end of dissections. Brains were fixed in Schneider + 4% PFA for 25 min at room temperature followed by three-times 20 min washes in washing solution (PBS1X [Thermo Fisher Scientific, 14200083] + 0.3% Triton-X-100 [Sigma-Aldrich, T8787] + 5 mg/mL BSA [Euromedex, 04-100-812-E]). Saturation was realized over 1 h in blocking solution (washing solution + 4% NGS [Sigma-Aldrich, G9023]). Brains were incubated in primary antibodies overnight at 4°C with rabbit anti-GFP (1:200 [Thermo Fisher Scientific, A6455]), mouse anti-Elav (1:400 [Developmental Studies Hybridoma Bank, 7E8A10]) or rabbit anti-tyrosine-hydroxylase (1:500 [Sigma-Aldrich, AB152]) diluted in blocking solution. Brains were washed three times for 20 min each. before secondary antibodies incubation for 3 h at room temperature with anti-Rabbit-A488 (1:400 [Thermo Fisher Scientific, A-11008]) or anti-Mouse-A546 (1:400 [Thermo Fisher Scientific, A-11030]) diluted in blocking solution. Finally, brains washed three times for 20 min each and mounted in Vectashield (Eurobio Scientific, H-1000) on bridge slides. Confocal microscopy was performed using a Zeiss LSM800 microscope.

SING Assay

Locomotion ability was measured using SING assay. Females were preferred as they perform more robustly the locomotion assay. For each condition, 6 groups of 18 adult females were harvested within one day of adult hatching. 30 min before the SING assay, flies were left at room temperature for habituation. Each group was then placed in a column (25 cm long and 1 cm in diameter). First, flies underwent three training sessions in which they were gently tapping down and let climb to the top of the column. Second, flies were assayed by gently tapping them down and counting the number of flies having reached the top of the column (n_{up} [above 18 cm]) and those staying at the bottom end (n_{down} [below 2.5 cm]) after 30 sec. Each group was

assayed 3 times with 2 min intervals. The mean of the 3-times assay was used to calculate a performing index: $\frac{1}{2}[(n_{tot}+n_{up}-n_{down})/n_{tot}]$ where n_{tot} is the total number of flies. For each condition, the result is the mean ±SEM of the 6 groups.

Fertility Assay

The fertility assay was performed by quantifiying the laid eggs from fertilized females of different genotypes. For that, two crosses were set up with ten 1- to 3-day-old control males and ten 1- to 3-day-old control or *dwdr45* KO virgin females for 3 day at 25°C. Flies were then transferred to a fertility assay chamber with laying medium (300 mL H2O, 100 mL grape juice, 10 g sucrose [Euromedex, 200-301-B], 9 g agar [VWR International, 20768.235], 0.6 g nipagine [Sigma-Aldrich, H3647]). Twice per day and for five days, laid eggs were counted, and a new medium was provided. After 48 h, the number of unhatched eggs was counted: yellow eggs were considered unfertilized, dark eggs were considered as eggs with embryonic development disturbing. The number of hatched eggs corresponds to the difference between laid eggs and unhatched eggs.

Lifespan Analysis

For lifespan analysis, 6 vials of 20 adult females per condition were harvested within one day of adult hatching. Every two or three days, flies were transferred to a new vial and longevity was scored by counting the number of dead flies. Flies that escaped from the vial were recorded as censored. The Kaplan-Meier curve represents the percentage of surviving flies depending on time. Statistical analyses were performed on R Software using 'survival' package. Cox test was performed to allow for comparison multiple conditions based on hazard ratio that corresponds to the probability of fly death event apparition.

Western Blot Analysis

Fly heads (n=10) were mixed in 50 µL of Laemmli buffer 1X (Sigma-Aldrich, S3401) and boiled for 5 min before freezing. Proteins were separated by sodium dodecyl sulfate-polyacrylamide gel electrophoresis (BIO-RAD, 4568093) at 100 V during 1 h before transferring on polyvinylidene difluoride membrane (Thermo Fisher Scientific, 88518) at 25 V overnight at 4°C. Membrane was washed three times for 5 min each in Tris-Buffered Saline (TBS) + 0.1% Tween-20 (Sigma-Aldrich, P1379) before 10 min saturation in blocking solution (TBS1X + 0.1% Tween-20 + 5% BSA). The primary antibodies incubation was performed overnight at 4°C with mouse anti-α-Tubulin (1:2000 [Sigma-Aldrich, T6199]), rabbit anti-Gabarap (1:2000 [abcam, ab109364]), rabbit anti-Ref(2)P (1:1000 [abcam, ab178440]), rabbit anti-Fer1HCH (1:500) or rabbit anti-Fer2LCH (1:500) (Gift from Fanis Missirlis, [41]) diluted in blocking solution. The membrane was washed three times for 5 min before secondary antibodies incubation 1 h at

room temperature with anti-Mouse-A488 (1:10 000 [Thermo Fisher Scientific, A-11001]) and anti-Rabbit-A546 (1:10 000 [Thermo Fisher Scientific, A-11035]) diluted in blocking solution. The membrane was finally washed three times for 5 min each before fluorescence monitoring using ChemiDoc MP Imaging System (Bio-RAD). Analysis was realized by quantification of band fluorescence intensity using ImageLab software (BIO-RAD).

Ferrozine Assay

Ferrozine assays were adapted from Riemer et al., [42]. Briefly, the whole bodies of 3 flies were ground in 125 µL of 50mM NaOH and kept for 2 h at 4°C on a rotor. 100 µL of lysate and 100 µL of 10 mM HCl were mixed before adding 100 µL of the iron-releasing reagent (50 µL of 1.4 M HCl + 50 µL of 4.5% KMnO4 [Sigma-Aldrich, 223468] diluted in H2O). Samples were heated 2 h at 60°C before cooling at room temperature. Finally, 20 µL of iron-detection solution (6.5 mM ferrozine [Sigma-Aldrich, 82940], 6.5 mM neocuproine [Sigma-Aldrich, 72090], 2.5 mM ammonium acetate [Sigma-Aldrich, A1542], 1 M ascorbic acid [Sigma-Aldrich, A5960] diluted in H2O) were added. Absorbance was read in triplicate on 96-well plate at 560 nm. The iron concentration was determined by using a standard curve and normalized against the protein concentration measured using the Bradford assay on 5 µL of lysate. For each condition, quadruplicates were performed.

Adult retina immunostaining

For each condition, 8 retina of 8-day-old adult female flies were dissected in Schneider medium and stored in Schneider + 1% PFA on ice until end of dissections. Brains were fixed in Schneider + 4% PFA for 20 min at room temperature followed by three-times 15 min washes in washing solution (PBS1X + 0.3% Triton-X-100 + 5 mg/mL BSA). Saturation was realized over 30 min in blocking solution (washing solution + 4% NGS). Retina were incubated in primary antibodies overnight at 4°C with rabbit anti-GFP (1:200 [Thermo Fisher Scientific, A6455]) or rabbit anti-Ref(2)P (1:400 [provided from S. Gaumer]) diluted in blocking solution. Retina were washed three times for 15 min each before secondary antibodies incubation for 2 h at room temperature with anti-Rabbit-A488 and Phalloidin-Rhodamine (1:400 [Thermo Fisher Scientific, R415]) diluted in blocking solution. Finally, brains were washed three times for 15 min each mounted in Vectashield on bridge slides. Confocal microscopy was done using a Zeiss LSM800 microscope.

Adult retina immunostaining by cryosection

For each condition, 6 fly heads were cut in PBS1X and placed in OCT (Electron Microscopy Sciences, 62550) before 1h freezing in dry ice. 10 µm slices were cut using HM525 NX Cryostat and collected on superfrost slides (VWR International, 48404-476). Slides were dried

15 min before fixation in PBS1X + 4% PFA for 1 h at room temperature. Slides were briefly washed in three successive PBS1X baths before saturating in blocking solution (PBS1X + 0.3% Triton-X-100 + 1% BSA) over 30 min. Primary antibody incubation was realized for 1h at room temperature with rabbit anti-GFP (1:400) or rabbit anti-Ref(2)P (1:400 [provided from S. Gaumer]) diluted in blocking solution. Slides were briefly washed in three successive PBS1X baths before secondary antibody incubation for 1 h with anti-rabbit-A647 (1:400 [Thermo Fisher Scientific, A-31573]) diluted in blocking solution. Finally, slides were briefly washed in three successive PBS1X baths before mounting in Vectashield with DAPI (Eurobio Scientific, H-1200). Confocal microscopy was performed using a Zeiss LSM800 microscope.

Statistical Analyses

Statistical analyses were performed in JAMOVI, using R software. Samples were compared through one-way or two-way ANOVA depending on number of parameters. In addition, when ANOVA indicates a significant difference, post-hoc tests were performed using different corrections depending on variance's homogeneity: Tukey's correction for homoscedasticity or Games-Howell's correction for heteroscedasticity. On graphs, data are reported as the means ± standard error of mean (SEM) of three experiments unless otherwise noted.

Acknowledgments:

We are very grateful to the patient associations and funders who supported this work including Autour du BPAN, BPAN France, Groupama science foundation, Million Dollar Bike Ride to MC, LW and BM. SA was supported by a fellowship from the French Ministry of Higher Education and Research. RI was supported by a Marie Sklodowsa-Curie Action fellowship. We thank JORISS funding to BM and LL and the China Scholarship Council (CSC) to HJ. We thank our colleagues from the fly community and fly stock centers for providing fly stocks and antibody used in this study. We thank the Loppin team (B. Horard, LBMC) fo their help with fertility experiments. We thank the imaging LYMIC-PLATIM and the fly ARTHRO-TOOLS facilities (SFR Biosciences, Lyon). This article is dedicated to Dr Francine Côté, who always supported the fly as a great model to advance BPAN research.

References

1. Haack TB, Hogarth P, Kruer MC, et al. Exome sequencing reveals de novo WDR45 mutations causing a phenotypically distinct, X-linked dominant form of NBIA. Am J Hum Genet. 2012 Dec 7;91(6):1144-9. doi: 10.1016/j.ajhg.2012.10.019. PubMed PMID: 23176820; PubMed Central PMCID: PMCPMC3516593. eng.
2. Cong Y, So V, Tijssen MAJ, et al. WDR45, one gene associated with multiple neurodevelopmental disorders. Autophagy. 2021 Apr 12:1-16. doi: 10.1080/15548627.2021.1899669. PubMed PMID: 33843443; eng.
3. Proikas-Cezanne T, Haas ML, Pastor-Maldonado CJ, et al. Human WIPI beta-propeller function in autophagy and neurodegeneration. FEBS Lett. 2024 Jan;598(1):127-139. doi: 10.1002/1873-3468.14782. PubMed PMID: 38058212.
4. Zhu Y, Fujimaki M, Snape L, et al. Loss of WIPI4 in neurodegeneration causes autophagy-independent ferroptosis. Nat Cell Biol. 2024 Apr;26(4):542-551. doi: 10.1038/s41556-024-01373-3. PubMed PMID: 38454050; PubMed Central PMCID: PMCPMC11021183.
5. Papandreou A, Singh N, Gianfrancesco L, et al. Cardiac glycosides restore autophagy flux in an iPSC-derived neuronal model of WDR45 deficiency. bioRxiv. 2024 Jun 17. PubMed PMID: 37745522; eng.
6. Mollereau B, Hayflick SJ, Escalante R, et al. A burning question from the first international BPAN symposium: is restoration of autophagy a promising therapeutic strategy for BPAN? Autophagy. 2023 Dec;19(12):3234-3239. doi: 10.1080/15548627.2023.2247314. PubMed PMID: 37565733; PubMed Central PMCID: PMCPMC10621268.
7. Napoletano F, Baron O, Vandenabeele P, et al. Intersections between Regulated Cell Death and Autophagy. Trends Cell Biol. 2019 Jan 18;9(4):323-338. doi: 10.1016/j.tcb.2018.12.007. PubMed PMID: 30665736; eng.
8. Simonsen A, Cumming RC, Brech A, et al. Promoting basal levels of autophagy in the nervous system enhances longevity and oxidant resistance in adult Drosophila. Autophagy. 2007 Feb;4(2):176-84. PubMed PMID: 18059160; eng.
9. Papandreou A, Singh N, Gianfrancesco L, et al. Cardiac glycosides restore autophagy flux in an iPSC-derived neuronal model of WDR45 deficiency. Elife. 2024. doi: 10.7554/eLife.91725.2.
10. Wan H, Wang Q, Chen X, et al. WDR45 contributes to neurodegeneration through regulation of ER homeostasis and neuronal death. Autophagy. 2019 Jun 23:1-17. doi: 10.1080/15548627.2019.1630224. PubMed PMID: 31204559; eng.
11. Wynn DP, Pulst SM. A novel WDR45 mutation in a patient with beta-propeller protein-associated neurodegeneration. Neurology Genetics. 2017 Feb;3(1):e124. doi: 10.1212/nxg.0000000000000124. PubMed PMID: 27957548; PubMed Central PMCID: PMCPMC5141522. eng.
12. Wilson JL, Gregory A, Kurian MA, et al. Consensus clinical management guideline for beta-propeller protein-associated neurodegeneration. Dev Med Child Neurol. 2021 Aug 4. doi: 10.1111/dmcn.14980. PubMed PMID: 34347296; eng.
13. Biagosch CA, Vidali S, Faerberboeck M, et al. A comprehensive phenotypic characterization of a whole-body Wdr45 knock-out mouse. Mamm Genome. 2021 May 27. doi: 10.1007/s00335-021-09875-3. PubMed PMID: 34043061; eng.
14. Zhao YG, Sun L, Miao G, et al. The autophagy gene Wdr45/Wipi4 regulates learning and memory function and axonal homeostasis. Autophagy. 2015;11(6):881-90. doi:

10.1080/15548627.2015.1047127. PubMed PMID: 26000824; PubMed Central PMCID: PMCPMC4502681. eng.
15. McGurk L, Berson A, Bonini NM. Drosophila as an In Vivo Model for Human Neurodegenerative Disease. Genetics. 2015 Oct;201(2):377-402. doi: 10.1534/genetics.115.179457. PubMed PMID: 26447127; eng.
16. St Johnston D. The art and design of genetic screens: Drosophila melanogaster. Nat Rev Genet. 2002 Mar;3(3):176-88. doi: 10.1038/nrg751. PubMed PMID: 11972155; eng.
17. Tang X, Zhou B. Ferritin is the key to dietary iron absorption and tissue iron detoxification in Drosophila melanogaster. Faseb j. 2013 Jan;27(1):288-98. doi: 10.1096/fj.12-213595. PubMed PMID: 23064556; eng.
18. Rosas-Arellano A, Vasquez-Procopio J, Gambis A, et al. Ferritin Assembly in Enterocytes of Drosophila melanogaster. Int J Mol Sci. 2016;17(2). doi: 10.3390/ijms17020027. PubMed PMID: 26861293; eng.
19. Davie K, Janssens J, Koldere D, et al. A Single-Cell Transcriptome Atlas of the Aging Drosophila Brain. Cell. 2018 Aug 9;174(4):982-998.e20. doi: 10.1016/j.cell.2018.05.057. PubMed PMID: 29909982; PubMed Central PMCID: PMCPMC6086935. eng.
20. Allen AM, Neville MC, Birtles S, et al. A single-cell transcriptomic atlas of the adult Drosophila ventral nerve cord. Elife. 2020 Apr 21;9. doi: 10.7554/eLife.54074. PubMed PMID: 32314735; PubMed Central PMCID: PMCPMC7173974.
21. Fouillet A, Levet C, Virgone A, et al. ER stress inhibits neuronal death by promoting autophagy. Autophagy. 2012 Jun;8(6):915-26. doi: 10.4161/auto.19716. PubMed PMID: 22660271; eng.
22. Sun J, Xu AQ, Giraud J, et al. Neural Control of Startle-Induced Locomotion by the Mushroom Bodies and Associated Neurons in Drosophila. Frontiers in systems neuroscience. 2018;12:6. doi: 10.3389/fnsys.2018.00006. PubMed PMID: 29643770; PubMed Central PMCID: PMCPMC5882849. eng.
23. Feany MB, Bender WW. A Drosophila model of Parkinson's disease. Nature. 2000 Mar 23;404(6776):394-8. PubMed PMID: 10746727.
24. Seibler P, Burbulla LF, Dulovic M, et al. Iron overload is accompanied by mitochondrial and lysosomal dysfunction in WDR45 mutant cells. Brain. 2018 Oct 1;141(10):3052-3064. doi: 10.1093/brain/awy230. PubMed PMID: 30169597; PubMed Central PMCID: PMCPMC7190033.
25. Xiong Q, Li X, Li W, et al. WDR45 Mutation Impairs the Autophagic Degradation of Transferrin Receptor and Promotes Ferroptosis. Front Mol Biosci. 2021;8:645831. doi: 10.3389/fmolb.2021.645831. PubMed PMID: 34012978; PubMed Central PMCID: PMCPMC8126626. eng.
26. Tornero-Écija A, Tábara LC, Bueno-Arribas M, et al. A Dictyostelium model for BPAN disease reveals a functional relationship between the WDR45/WIPI4 homolog Wdr45l and Vmp1 in the regulation of autophagy-associated PtdIns3P and ER stress. Autophagy. 2021 Jul 27:1-17. doi: 10.1080/15548627.2021.1953262. PubMed PMID: 34328055; eng.
27. Klionsky DJ, Abdel-Aziz AK, Abdelfatah S, et al. Guidelines for the use and interpretation of assays for monitoring autophagy (4th edition)(1). Autophagy. 2021 Jan;17(1):1-382. doi: 10.1080/15548627.2020.1797280. PubMed PMID: 33634751; PubMed Central PMCID: PMCPMC7996087. eng.

28. Robin M, Issa AR, Santos CC, et al. Drosophila p53 integrates the antagonism between autophagy and apoptosis in response to stress. Autophagy. 2019 Dec 19;15(5):771-784. doi: 10.1080/15548627.2018.1558001. PubMed PMID: 30563404; eng.
29. Nisoli I, Chauvin JP, Napoletano F, et al. Neurodegeneration by polyglutamine Atrophin is not rescued by induction of autophagy. Cell Death Differ. 2010 Mar 26;17(10):1577-87. PubMed PMID: 20339376.
30. Bartlett BJ, Isakson P, Lewerenz J, et al. p62, Ref(2)P and ubiquitinated proteins are conserved markers of neuronal aging, aggregate formation and progressive autophagic defects. Autophagy. 2011 Jun;7(6):572-83. PubMed PMID: 21325881; eng.
31. Jain A, Rusten TE, Katheder N, et al. p62/Sequestosome-1, Autophagy-related Gene 8, and Autophagy in Drosophila Are Regulated by Nuclear Factor Erythroid 2-related Factor 2 (NRF2), Independent of Transcription Factor TFEB. J Biol Chem. 2015 Jun 12;290(24):14945-62. doi: 10.1074/jbc.M115.656116. PubMed PMID: 25931115; PubMed Central PMCID: PMCPMC4463441. eng.
32. Juhasz G, Erdi B, Sass M, et al. Atg7-dependent autophagy promotes neuronal health, stress tolerance, and longevity but is dispensable for metamorphosis in Drosophila. Genes Dev. 2007 Dec 1;21(23):3061-6. doi: 10.1101/gad.1600707. PubMed PMID: 18056421; eng.
33. Kim M, Sandford E, Gatica D, et al. Mutation in ATG5 reduces autophagy and leads to ataxia with developmental delay. Elife. 2016 Jan 26;5. doi: 10.7554/eLife.12245. PubMed PMID: 26812546; PubMed Central PMCID: PMCPMC4786408.
34. Bjedov I, Cocheme HM, Foley A, et al. Fine-tuning autophagy maximises lifespan and is associated with changes in mitochondrial gene expression in Drosophila. PLoS Genet. 2020 Nov;16(11):e1009083. doi: 10.1371/journal.pgen.1009083. PubMed PMID: 33253201; PubMed Central PMCID: PMCPMC7738165.
35. Wang T, Lao U, Edgar BA. TOR-mediated autophagy regulates cell death in Drosophila neurodegenerative disease. J Cell Biol. 2009 Aug 31. PubMed PMID: 19720874.
36. Aring L, Choi EK, Kopera H, et al. A neurodegeneration gene, WDR45, links impaired ferritinophagy to iron accumulation. J Neurochem. 2022 Feb;160(3):356-375. doi: 10.1111/jnc.15548. PubMed PMID: 34837396; PubMed Central PMCID: PMCPMC8811950.
37. Xiong Q, Sun H, Xing W, et al. WDR45 mutation dysregulates iron homeostasis by promoting the chaperone-mediated autophagic degradation of ferritin heavy chain in an ER stress/p38 dependent mechanism. Free Radic Biol Med. 2023 Mar 20;201:89-97. doi: 10.1016/j.freeradbiomed.2023.03.012. PubMed PMID: 36940732.
38. Ji C, Zhao H, Li D, et al. Role of Wdr45b in maintaining neural autophagy and cognitive function. Autophagy. 2020 Apr;16(4):615-625. doi: 10.1080/15548627.2019.1632621. PubMed PMID: 31238825; PubMed Central PMCID: PMCPMC7138210. eng.
39. Ji C, Zhao H, Li D, et al. Role of Wdr45b in maintaining neural autophagy and cognitive function. Autophagy. 2019 Jun 25:1-11. doi: 10.1080/15548627.2019.1632621. PubMed PMID: 31238825; eng.
40. Mollereau B, Wernet MF, Beaufils P, et al. A green fluorescent protein enhancer trap screen in Drosophila photoreceptor cells. Mech Dev. 2000;93(1-2):151-160. PubMed Central PMCID: PMC 10781948.
41. Missirlis F, Holmberg S, Georgieva T, et al. Characterization of mitochondrial ferritin in Drosophila. Proc Natl Acad Sci U S A. 2006 Apr 11;103(15):5893-8. PubMed PMID: 16571656.

42. Riemer J, Hoepken HH, Czerwinska H, et al. Colorimetric ferrozine-based assay for the quantitation of iron in cultured cells. Analytical biochemistry. 2004 Aug 15;331(2):370-5. doi: 10.1016/j.ab.2004.03.049. PubMed PMID: 15265744.

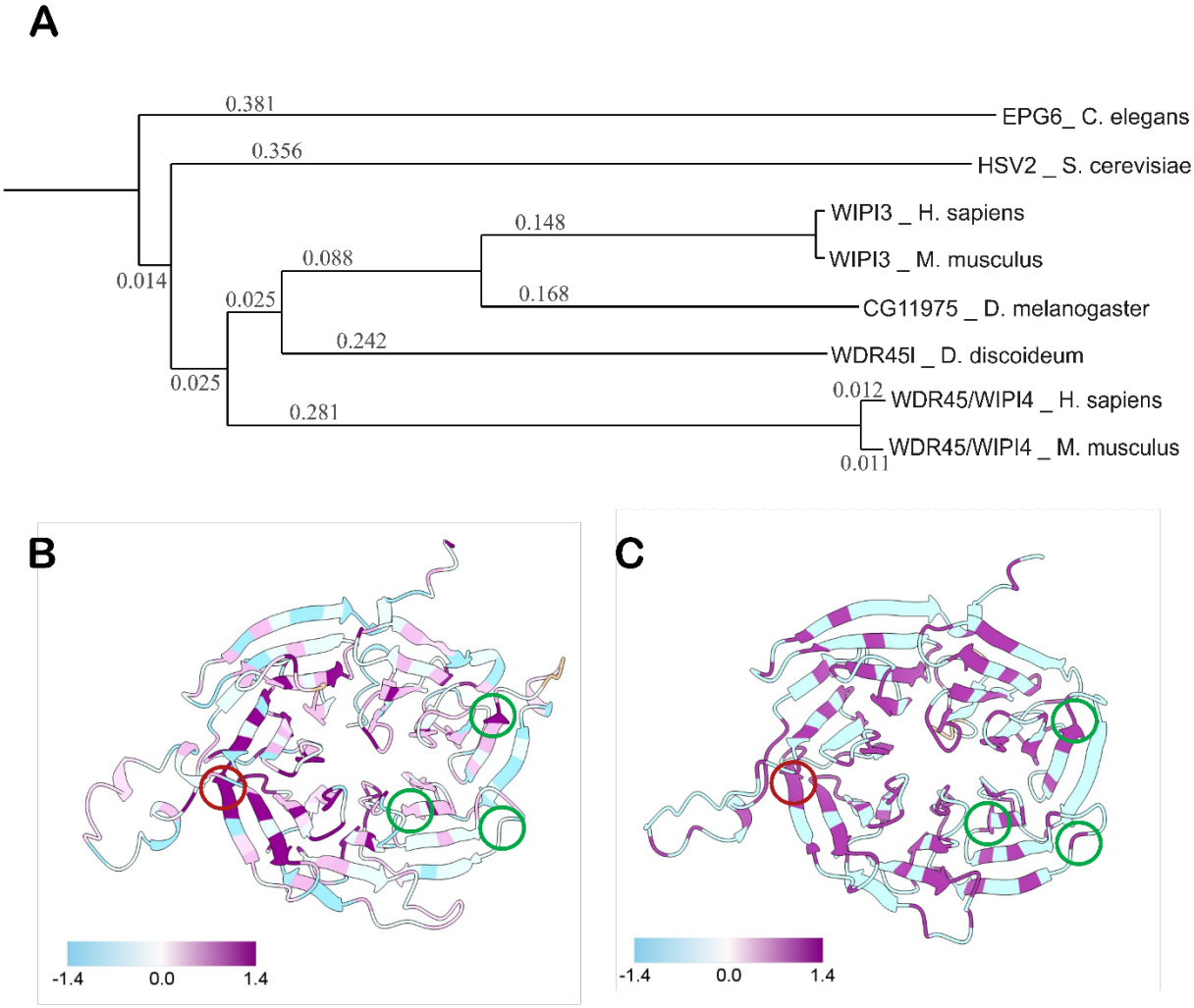

Figure 1. CG11975/dWDR45, the *Drosophila* homolog of WDR45.

(**A**) Phylogenetic tree based on amino acids analysis of hWDR45 and its homolog in *Homo sapiens*, *Mus musculus*, *Drosophila melanogaster*, *Dictyostelium discoideum* and *Saccharomyces cerevisiae*. Branch's length represents evolutive distance. (**B**) Chimeric representation of hWDR45 protein colorizing on conservation index with its orthologs. Phosphoinositide binding domain and ATG2 binding sites are highlighted with red and green circles, respectively. (**C**) Chimeric representation of dWDR45 colorizing on conservation index with hWDR45. Phosphoinositide binding domain and ATG2 binding sites are highlighted with red and green circles, respectively.

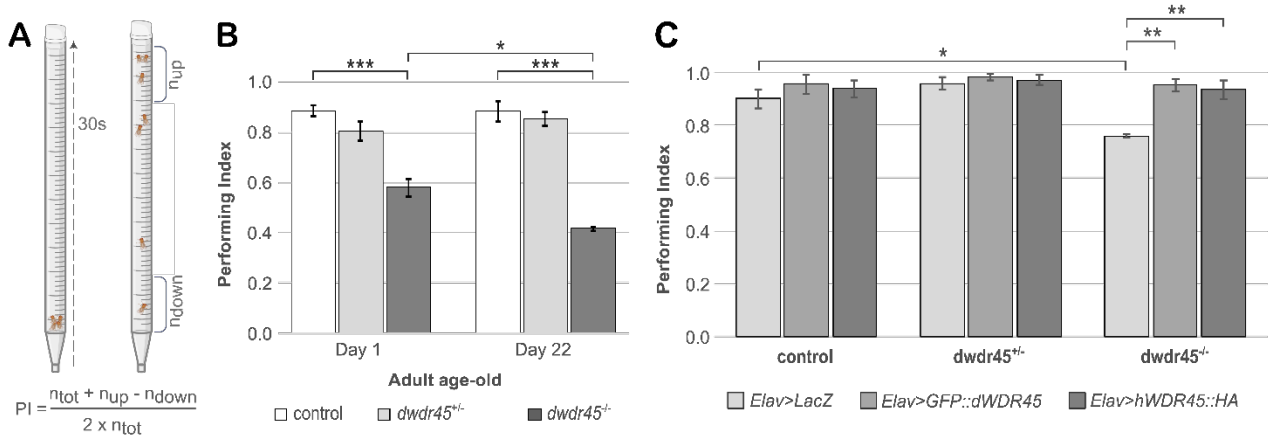

<u>Figure 2. *dwdr45* KO flies exhibit a locomotion defect, which is rescued by the neuronal expression of dWDR45 or human WDR45.</u>

(**A**) Schematic representation of the SING assay. (**B**) Representative experiment of three SING assays realized in 1- or 22-day-old adult control (w^{1112}) , heterozygous *dwdr45* KO or homozygous *dwdr45* KO flies. Statistical analyses were carried out with ANOVA2/post-hoc test: *p-value<0.05, **p-value<0.01 and ***p-value<0.001**.** (**C**) SING assays were realized in 8-day-old adult control, heterozygous *dwdr45* KO or homozygous *dwdr45* KO flies expressing LacZ, GFP::dWDR45 or human WDR45::HA with the pan-neuronal *Elav* driver. Statistical analyses were carried out in three independent experiments with ANOVA2/post-hoc test: *p-value<0.05 and **p-value<0.01.

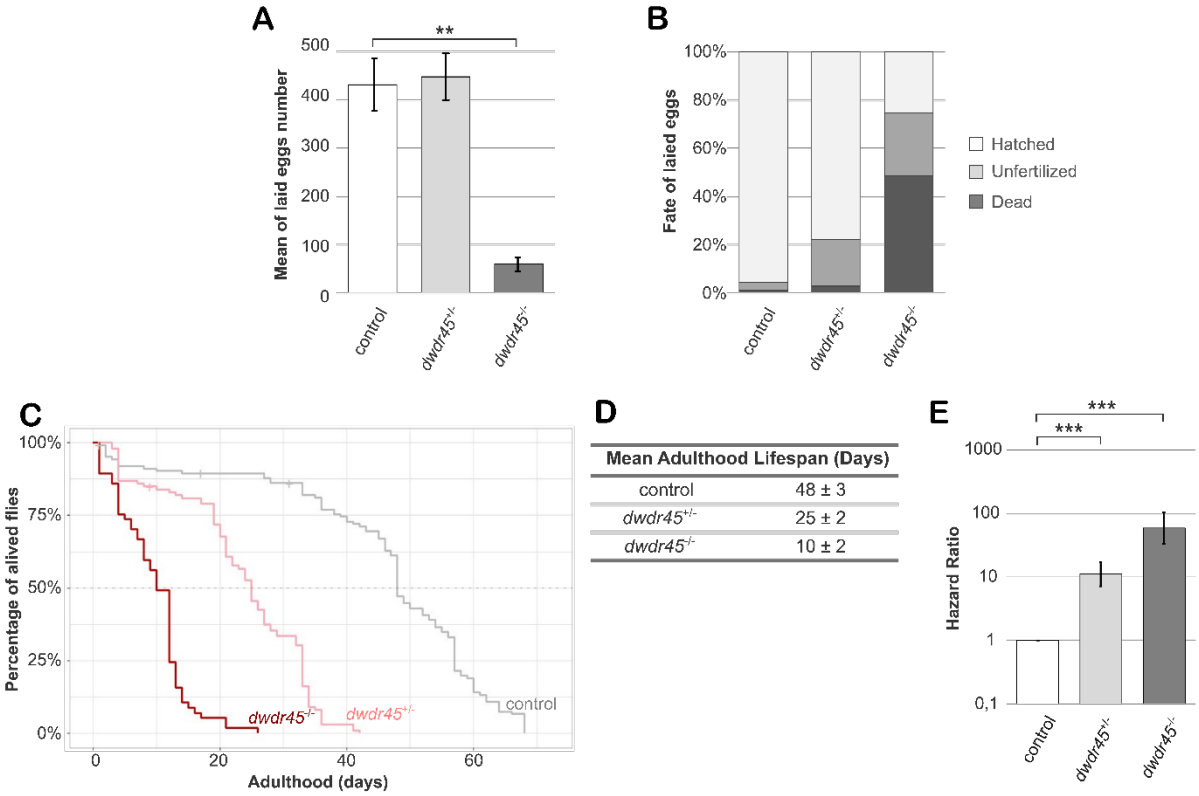

Mean Adulthood Lifespan (Days)	
control	48 ± 3
dwdr45$^{+/-}$	25 ± 2
dwdr45$^{-/-}$	10 ± 2

Figure 3. *dwdr45* is required for fertility and lifespan maintenance.

(**A and B**) Fertility was assayed by (**A**) quantifying the number of eggs laid and (**B**) their fate unfertilized, dead and subsequent larval hatching. Control or *dwdr45* KO female flies were crossed with control male flies. Statistical analyses were carried out in three independent experiments with ANOVA1/post-hoc: **p-value<0.01. (**C, D and E**) Lifespan assays were realized in control or *dwdr45* KO female flies with Kaplan-Meier analysis. (**C**) A representative lifespan experiment out of three independent experiments is shown. (**D**) The mean adulthood lifespan and (**E**) the hazard ratio (probability of fly death event) are shown in the indicated genetic backgrounds. Statistical analyses were carried out with Coxph test: ***p-value<0.001.

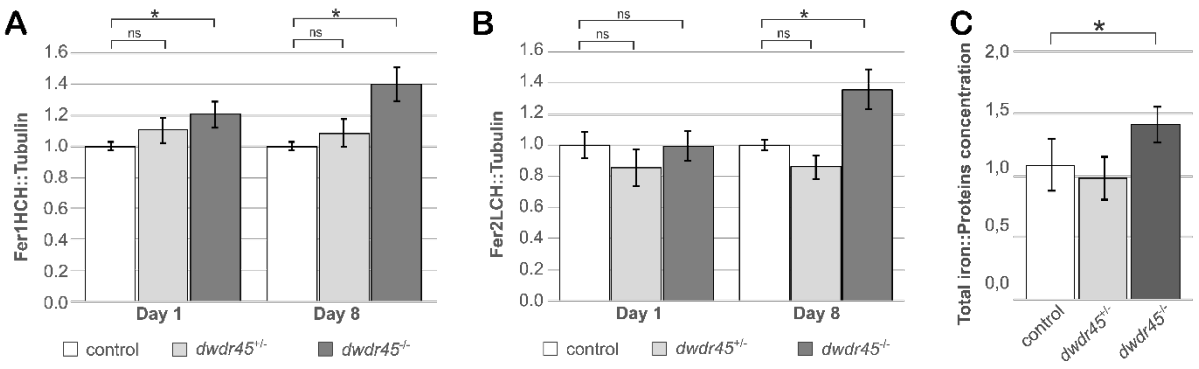

Figure 4. *dwdr45* is required for iron homeostasis.

(**A**) Fer1HCH and (**B**) Fer2LCH protein levels were quantified by western blotting in 1- and 8-day-old adult control, heterozygous or homozygous *dwdr45* KO flies. Ratio of ferritin over tubulin protein levels are normalized to control flies. Statistical analyses were realized in three independent experiments with ANOVA2/post-hoc test: ns: no-significant, *p-value<0.05. (**C**) Ratio of iron on protein concentration was quantified by a ferrozine assay in 1-day-old adult control or *dwdr45* KO flies. Statistical analyses were carried out in three independent experiments with ANOVA1/post-hoc test: *p-value<0.05.

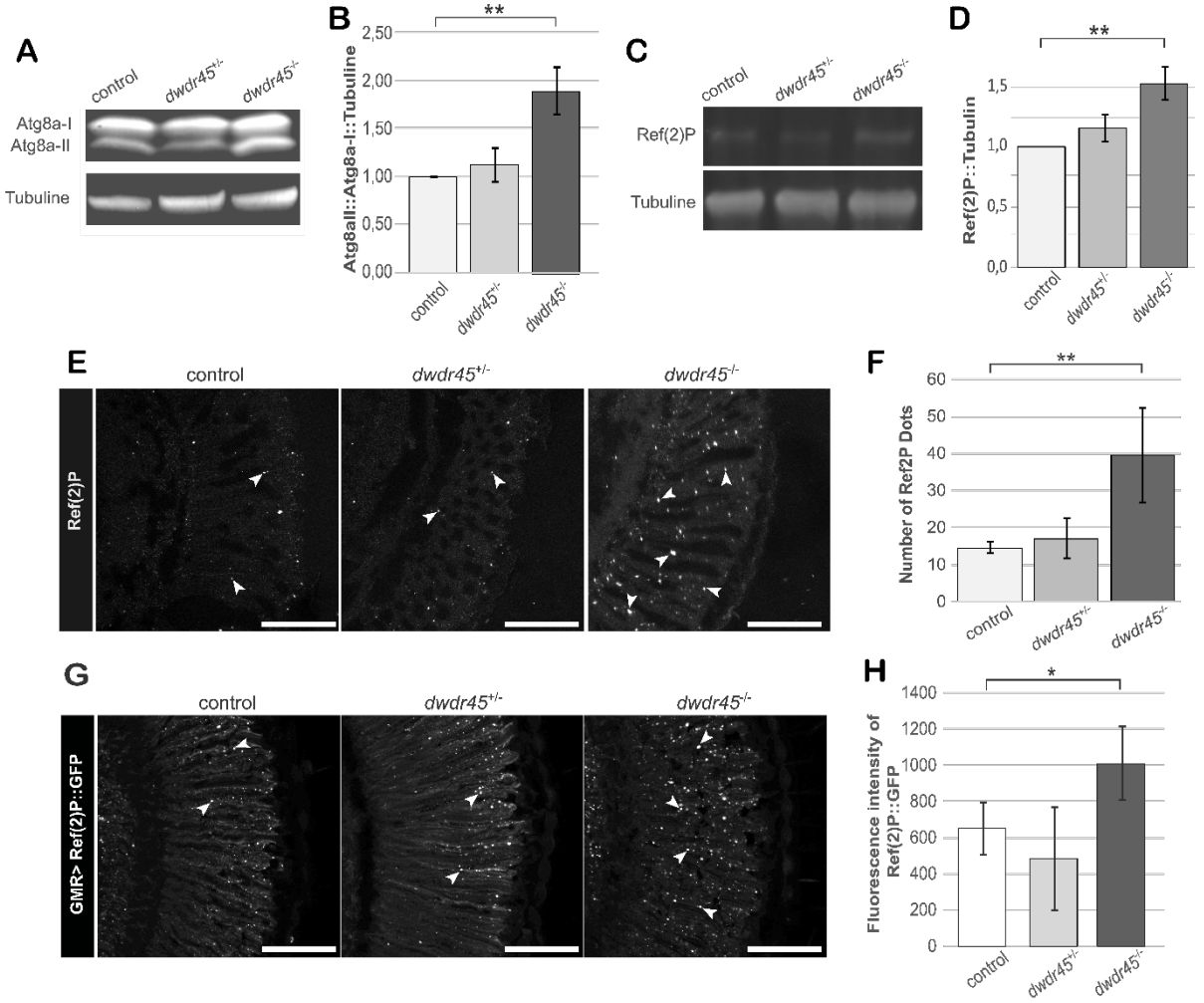

Figure 5. *dwdr45* is required for autophagy flux maintenance.

(**A)** Atg8a-II/Atg8a-I proteins are detected by western blotting in 8-day-old adult control and homozygous or heterozygous *dwdr45* KO flies. (**B**) The ratio of Atg8a-II/Atg8a-I relative to tubulin protein levels is normalized to control flies. Statistical analyses were carried out in three independent experiments with ANOVA1/post-hoc test: **p-value<0.01. (**C**) Ref(2)P protein is detected by western blotting in 8-day-old adult control and homozygous or heterozygous *dwdr45* KO flies. (**D**) Ref(2)P relative to tubulin protein levels is normalized to control flies. Statistical analyses were carried out in three independent experiments with ANOVA1/post-hoc test: *p-value<0.05. (**E**) Immunolabelling of Ref(2)P protein in retina of 15-day-old adult control and homozygous or heterozygous *dwdr45* KO flies. (**F**) The number of Ref(2)P dots relative to retina surface area was quantified. Statistical analyses were carried out in three independent experiments with ANOVA1/post-hoc test: **p-value<0.01. Scale bars represent 50 µm. (**F**) Immunolabelling of GFP adult retina overexpressing Ref(2)P::GFP under the pan-retinal GMR driver in 15-day-old control or heterozygous or homozygous *dwdr45* KO flies. (**G**)

Quantification of GFP fluorescence. Statistical analyses were carried out in three independent experiments with ANOVA1/post-hoc test: *p-value<0.05. Scale bars represent 50 μm.

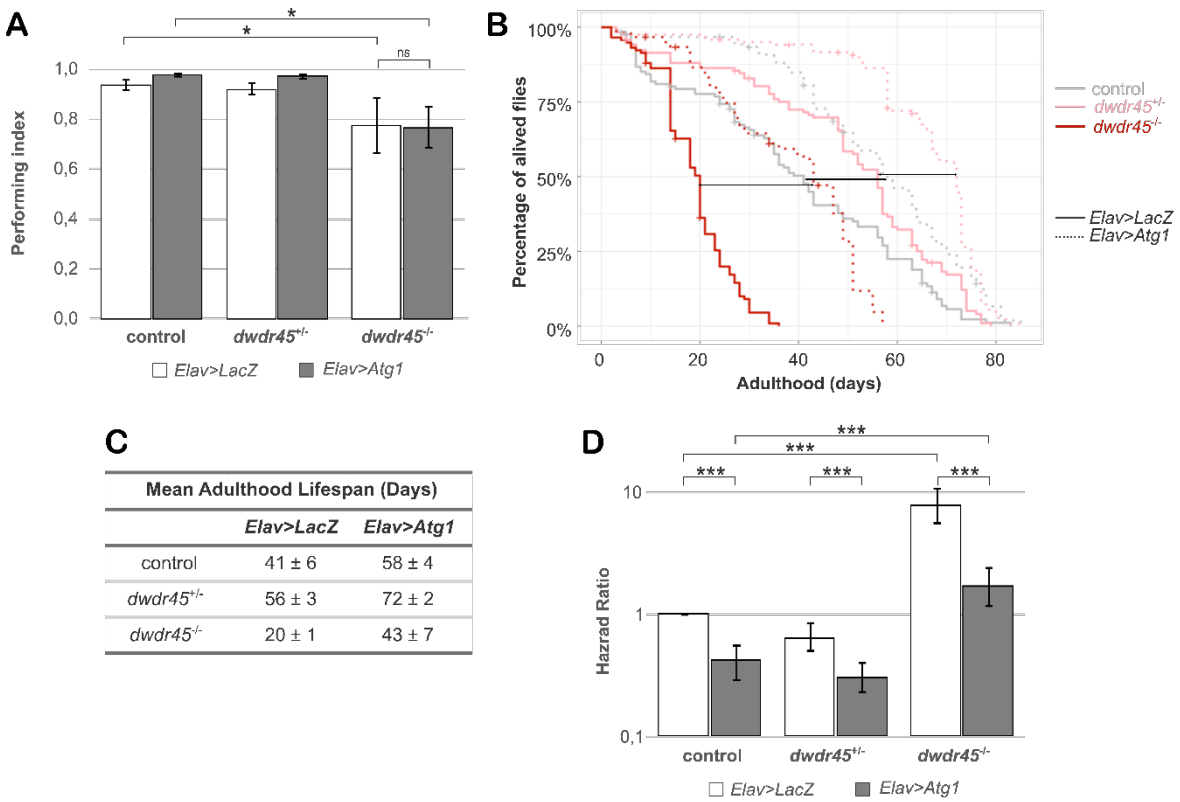

Mean Adulthood Lifespan (Days)		
	Elav>LacZ	*Elav>Atg1*
control	41 ± 6	58 ± 4
dwdr45$^{+/-}$	56 ± 3	72 ± 2
dwdr45$^{-/-}$	20 ± 1	43 ± 7

<u>Figure 6. Neuronal overexpression of Atg1 improves lifespan but not locomotion in *dwdr45* KO flies.</u>

Neuronal overexpression of LacZ or Atg1, under the pan-neuronal driver E*lav*, in control or heterozygous or homozygous *dwdr45* KO flies. (**A**) Locomotion SING assays were realized in 8-day-old adult flies. Statistical analyses were carried out on performing index in three independent experiments with ANOVA2/post-hoc test: ^{ns}non-significant, ***p-value<0.001. (**B**) Representative lifespan analysis out of three independent experiments is shown. (**C**) Associated mean adulthood lifespan and (**D**) hazard ratio (probability of fly death event). Statistical analyses carried out with Coxph test (***p-value<0.001) show that *dwdr45*$^{+/-}$ and dwdr45$^{-/-}$ have an increased hazard ratio compared to control flies. The reduction of hazard ratio induced by the overexpression of Atg1 is more pronounced in *dwdr45*$^{-/-}$ compared to control flies.